Laser Excitation of a Fracture Source for Elastic Waves

Thomas E. Blum* and Kasper van Wijk
Physical Acoustics Laboratory and Department of Geosciences, Boise State University, Boise, Idaho 83725, USA

Roel Snieder
Center for Wave Phenomena and Department of Geophysics, Colorado School of Mines, Golden, Colorado 80401, USA

Mark E. Willis†
ConocoPhillips Company, Houston, Texas 77079, USA.
(Received 2 September 2011; published 27 December 2011)

We show that elastic waves can be excited at a fracture inside a transparent sample by focusing laser light directly onto this fracture. The associated displacement field, measured by a laser interferometer, has pronounced waves that are diffracted at the fracture tips. We confirm that these are tip diffractions from direct excitation of the fracture by comparing them with tip diffractions from scattered elastic waves excited on the exterior of the sample. Being able to investigate fractures—in this case in an optically transparent material—via direct excitation opens the door to more detailed studies of fracture properties in general.

DOI: 10.1103/PhysRevLett.107.275501 PACS numbers: 62.30.+d, 62.25.Mn, 62.65.+k, 91.30.Bi

Introduction.—Being able to remotely sense the properties of fractures with elastic waves is of great importance in seismology [e.g., [1]] and nondestructive testing [e.g., [2]. For example, in geothermal and hydrocarbon reservoirs, it is very common to use hydraulic fracturing methods to attempt to increase the native permeability of the rocks above what is present in any naturally occurring fractures. The microseismic events associated with the fracturing process typically radiate seismic energy, which is recorded in nearby wells or at the surface. Much is left to be understood about the nature of such fractures and their relationship to elastic waves, but the scaling issues involved make numerical modeling a challenge. On the other hand, laboratory studies of fractures or faults are used to investigate their mechanical properties, such as stiffness [3], fracture slip rate, stress drop, or rupture propagation [4]. Typically, fractures under laboratory investigation are either on the surface of samples, or the result of new or growing fractures from an applied stress to induce fracture stick-slip creep [5,6]. Recently, Blum *et al.* [7] used noncontacting techniques to probe a fracture inside a clear sample to recover the fracture compliance. A high-powered laser excites the surface of the sample creating ultrasonic waves. These waves scatter from the fracture and are recorded at the surface of the sample with a laser interferometer [8]. Here, instead of only exciting the ultrasonic waves at the sample surface, we focus a pulsed infrared (IR) laser beam at the fracture location, turning it into an ultrasonic source. This technique makes it possible to measure the fracture response as a function of source energy, stress on the sample, or the laser beam size and location. By scanning the fracture with a focused IR laser beam it may be possible to measure spatial variations in the fracture properties and delineate barriers and asperities [9], concepts that are of great importance in earthquake dynamics, for example. A localized excitation, along the fracture, could also be used to excite interface waves traveling along the fracture [10,11] to probe for properties such as fault gouge or the fluids filling the fracture. Here, we illustrate the use of direct excitation of a fracture to investigate the elastic effective size of the fracture by means of tip diffractions. To date, these are most commonly studied on surface cracks [12].

Experiment.—We create a single disk-shaped fracture by focusing a high-power Q-switched Nd:YAG laser in a cylinder made of extruded Poly(methyl methacrylate) (PMMA), with a diameter of 50.8 mm and a height of 150 mm. The laser generates a short pulse ($\sim$ 20 ns) of IR light that is absorbed by the sample material at the focal point and converted into heat. The sudden thermal expansion generates sufficient stress to form a fracture inside the plastic material [13,14]. Anisotropy in the elastic moduli, caused by the extrusion process, results in a fracture with an orientation parallel to the cylindrical axis. The fracture studied here is approximately circular with a diameter of $\sim$7 mm (Fig. 1).

Elastic waves are excited at the surface of the sample by using the same high-power Q-switched Nd:YAG laser, operated at a much lower power, and with a partially focused beam. When an energy pulse from the laser hits an optically absorbing surface, part of that energy is absorbed and converted into heat. The resulting localized heating causes thermal expansion, which in turn results in elastic waves in the ultrasonic range [8].

Typically, the laser is focused on the outside of the sample—but as we explore in this Letter—the laser can

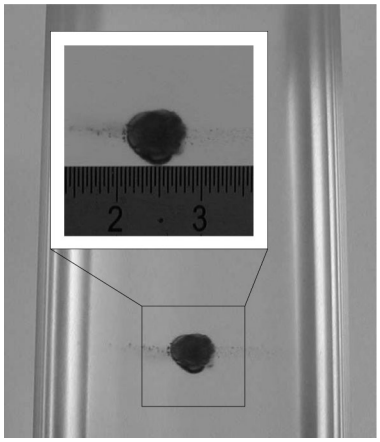

FIG. 1. Photograph of the laboratory sample and zoom around the disk-shaped fracture, with ruler units in cm. The sample is cut in half longitudinally to display the fracture without optical deformation by the curvature of the sample. The diameter of the fracture is ~7 mm, and the diameter of the cylinder is 50.8 mm.

also be focused inside the sample. In this case, the planar fracture has a visible contrast with the rest of the sample, seen as a darker region in Fig. 1. The Nd:YAG pulsed laser generates energy at a wavelength of 1064 nm, in the near IR. Therefore, we assume that the optical contrast due to the fracture is also present at the IR wavelength, leading to energy absorption and thermoelastic expansion at the fracture location.

We measure elastic displacement with a laser interferometer, based on a doubled Nd:YAG laser, generating a constant wave 250 mW beam at a wavelength of 532 nm. The light is split between a beam reflecting off the sample and one following a reference track inside the sensor. Two-wave mixing of the reflected and reference beams in a photorefractive crystal delivers a point measurement of the out-of-plane displacement field at the sample surface. The output is calibrated to give the absolute displacement in nanometers [7]. The frequency response is flat between 20 kHz and 20 MHz, and accurately detects displacements of the order of parts of angstroms. Since the PMMA sample is transparent for green light, we apply a reflective tape to the surface to reflect light back to the laser receiver.

The location of the noncontacting ultrasonic source and receiver are fixed in the laboratory frame of reference, but the PMMA sample is mounted on a rotational stage. The source-receiver angle δ (defined in Fig. 2) is therefore constant, here $\delta = 20°$, and only the orientation of the fracture with respect to the frame of reference, characterized by the angle θ, changes. Moreover, the source and receiver are focused on the sample in an (x, y) plane normal to the cylinder axis (z axis, Fig. 2). While anisotropic, as mentioned above, the extruded PMMA is transversely isotropic, and its elastic properties are therefore invariant with respect to the defined angles of interest.

By computer-controlled rotation of the stage, we measure the elastic field in the (x, y) plane for values of θ in

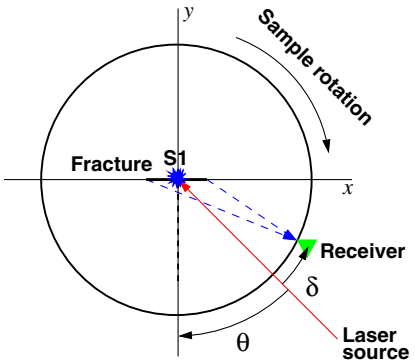

FIG. 2 (color online). Top view of the experimental setup for direct fracture excitation. The laser source beam (red) excites elastic waves (blue) at $S1$.

increments of 1°. The signal is digitized with 16-bit precision and a sampling rate of 100 MS/s (mega samples per second) and recorded on a computer acquisition board. For each receiver location, 256 waveforms are acquired and averaged after digitization.

Figure 3 shows the ultrasonic displacement field for the source $S1$ at the fracture for all recorded azimuths, after applying a 1–5 MHz band-pass filter. As defined in Fig. 2, the horizontal axis represents the angle θ between the normal to the fracture and the source direction. Electromagnetic interferences are generated by the high-power source laser when the light pulse is emitted, and leads to noise being recorded for short arrival times

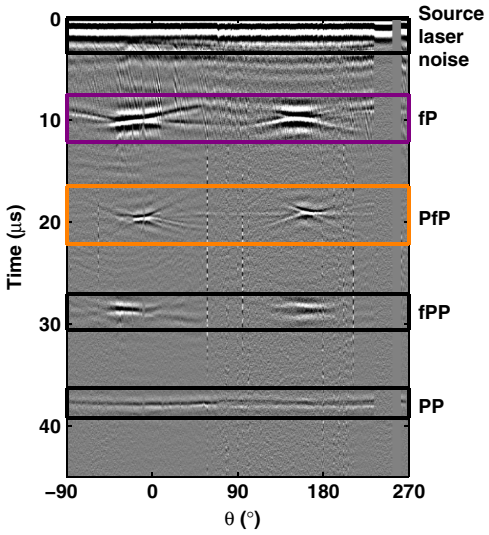

FIG. 3 (color online). Displacement field generated by excitation of the fracture. fP is the P wave generated at $S1$ and traveling directly to the receiver. PfP is the P wave generated at $S2$ and scattered by the fracture before reaching the receiver. fPP is the P wave generated at $S1$, traveling away from the receiver before bouncing back to the sample surface. Finally, PP is the P wave generated at $S2$, traveling across the sample and bouncing back to the receiver.

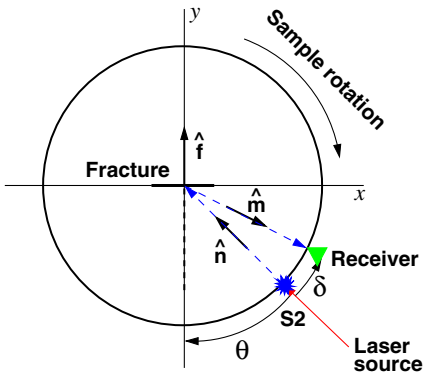

FIG. 4 (color online). Top view of the experimental setup for elastic-wave excitation at the sample surface. The laser source beam (red) excites elastic waves (blue) at $S2$.

(0–3 μs, highlighted in Fig. 2). The arrival at approximately 10 μs denoted fP corresponds to the wave field excited at the fracture. The fPP wave is excited at the fracture and reflects off the backside of the sample.

Next, we apply reflective tape where the source laser beam hits the sample surface at $S2$, increasing the IR light absorption at the surface and lowering the amount of energy reaching the fracture (Fig. 4). We repeat with this configuration the acquisition procedure used in the first experiment (Fig. 5). The PfP wave is generated at the surface of the sample, and then scattered by the fracture, while PP is scattered from the backside of the sample. PfP and PP phases are stronger than fP and fPP in Fig. 3, confirming that more of the thermoelastic expansion takes place at the surface of the cylinder.

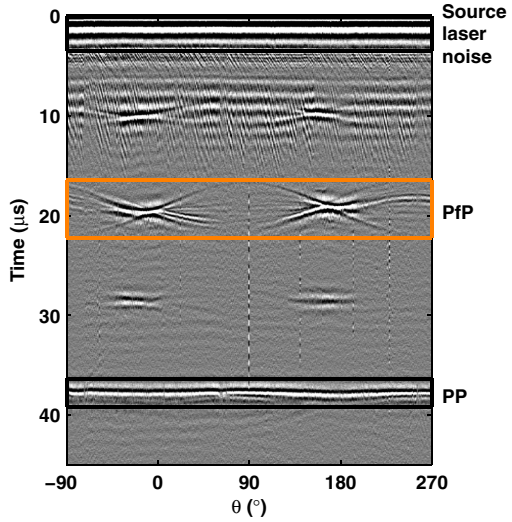

FIG. 5 (color online). Displacement field generated by excitation at the sample interface. Signal for $t < 3$ μs corresponds to noise generated by the laser source, and to the direct P wave traveling directly from the source $S1$ to the receiver. Other arrivals are defined in Fig. 3.

Fracture tip travel times.—The waves fP and PfP in Figs. 3 and 5 show a distinct lenticular pattern. For source angles $\theta = -10°$ and 170°, the PfP phase is a specular reflection, and the amplitude is a maximum. For intermediate angles, the scattered amplitude decreases [14]. Note splitting of the wave at intermediate angles into wavelets arriving before and after the specular reflection (see Fig. 6). These waves have the travel time and phase of waves diffracted by the crack tips. In particular, for $\theta = 70°$, the receiver is in the plane of the fracture, and therefore the travel time difference between the tips of the fracture the closest and the farthest to the receiver is largest (Fig. 4).

Equation 39 in [14] shows that the P to P scattered amplitude for a planar fracture in a linear-slip model under the Born approximation can be written in the frequency domain as a product of a scaling factor, a factor depending on the mechanical properties of the fracture and the propagation medium, and a *form factor* that depends on the fracture shape and the wave number change from the fracture scattering. Only this last factor carries time information. We show in the Appendix that the corresponding travel times are

$$t_{\text{tip-sc}} = \frac{R}{\alpha}\left(2 \pm \frac{a}{R}[\sin\theta(1+\cos\delta) + \sin\delta\cos\theta]\right), \quad (1)$$

where a is the radius of the fracture and R the radius of the cylinder. The P wave velocity is $\alpha = 2600$ m/s [14]. Figure 6 shows the PfP arrival overlain by the computed travel times from Eq. (1) with a fracture radius $a_{PfP} = 3.3$ mm.

For the arrival time of the fP wave that is excited at the fracture, we consider the geometry of rays originating from the fracture tips and traveling directly to the receiver. The ray paths are shown in Fig. 2. Using this geometry the travel time can be expressed as

$$t_{\text{tip-direct}} = \frac{\sqrt{a^2 \pm 2aR\sin(\theta) + R^2}}{\alpha}. \quad (2)$$

Because of the fact that the size of the fracture is small compared to the radius of the sample, this travel time is to leading order in a/R given by

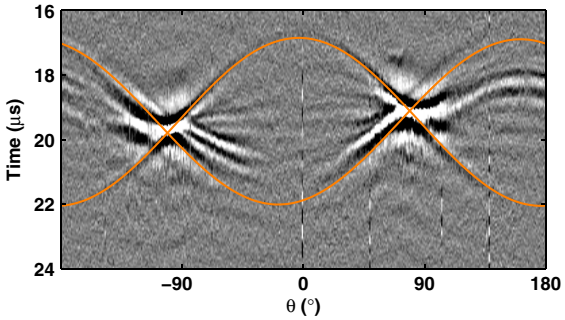

FIG. 6 (color online). Detailed view of the scattered (PfP) arrival. The solid (orange) curves represent the tip arrival times computed from Eq. (1).

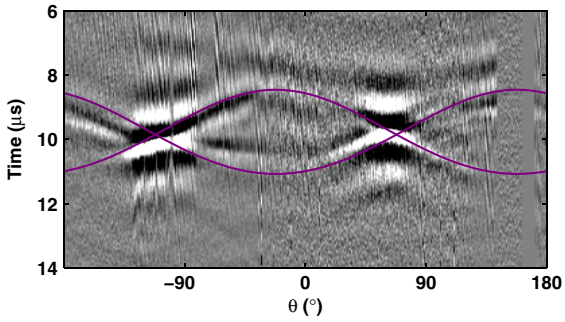

FIG. 7 (color online). Detailed view of the direct fracture excitation arrival. The solid (purple) curves represent the tip arrival times computed from Eq. (3).

$$t_{\text{tip-direct}} = \frac{R}{\alpha}\left(1 \pm \frac{a}{R}\sin(\theta)\right). \tag{3}$$

Figure 7 shows the fracture-source displacement field overlain with the tip arrival time (in purple) computed from Eq. (3). Just as in Fig. 6, the theoretical time for a radius $a_{fP} = 3.3$ mm agrees well with the arrival time of the fP wave, and the observed size in Fig. 1. The good agreement with the visually estimated radius confirms that the whole visually fractured area is mechanically discontinuous and capable of being excited by elastic waves.

Conclusions.—Laser-based ultrasonic techniques can not only excite and detect elastic waves at the surface, but can also be used to directly excite heterogeneities (such as fractures) inside an optically transparent sample. This result opens up possibilities for diagnosing the mechanical properties of fractures by directly exciting them. Here, we estimate the effective elastic size of the excited fracture. By scanning the fracture with a focused IR laser beam, it may be possible to measure spatial variations in the fracture properties and delineate barriers and asperities. These concepts are of great importance in earthquake dynamics, although hard to investigate in the field or numerically.

Appendix: Tip-diffraction times from form factor.—Equation 39 in [14] shows that the P to P scattered amplitude for a planar fracture in a linear-slip model under the Born approximation is

$$f_{P,P}(\hat{\mathbf{n}};\hat{\mathbf{m}}) = \frac{\omega^2}{4\pi\rho\alpha^4}AF[k_\alpha(\hat{\mathbf{n}}-\hat{\mathbf{m}})]\{\lambda^2\eta_N + 2\lambda\mu\eta_N[(\hat{\mathbf{n}}\cdot\hat{\mathbf{f}})^2 + (\hat{\mathbf{m}}\cdot\hat{\mathbf{f}})^2] + 4\mu^2(\eta_N-\eta_T)(\hat{\mathbf{n}}\cdot\hat{\mathbf{f}})^2(\hat{\mathbf{m}}\cdot\hat{\mathbf{f}})^2 + 4\mu^2\eta_T(\hat{\mathbf{n}}\cdot\hat{\mathbf{m}})(\hat{\mathbf{n}}\cdot\hat{\mathbf{f}})(\hat{\mathbf{m}}\cdot\hat{\mathbf{f}})\}, \tag{4}$$

where ω is the angular frequency, α the P-wave velocity, ρ the density of the material, λ and μ the Lamé parameters, A the surface area of the fracture, and η_N and η_T the normal and tangential compliances, respectively, for the linear-slip model. The unit vectors $\hat{\mathbf{n}}$ and $\hat{\mathbf{m}}$ denote the directions of incoming and outgoing waves, respectively, and $\hat{\mathbf{f}}$ is the unit vector normal to the fracture (see Fig. 4).

The prefactor $(\omega^2/4\pi\rho\alpha^4)A$ does not carry time information. The factor in curly brackets contains the angular dependence of the scattering amplitude, and depends only on the mechanical properties of the fracture η_N and η_T of the sample material, and on the directions of the incoming and outgoing waves relative to the fracture orientation. The form factor $F[k_\alpha(\hat{\mathbf{n}}-\hat{\mathbf{m}})]$ depends on the fracture size and shape, and contains travel time information. For the case of a circular fracture, the form factor can be expressed as [Eq. (33) in [14]]:

$$F[k_\alpha(\hat{\mathbf{n}}-\hat{\mathbf{m}})] = \frac{2}{k_\parallel a}J_1(k_\parallel a), \tag{5}$$

where a is the radius of the fracture, $k_\parallel$ the projection of the wave number change during the scattering onto the fracture plane, and J_1 the first order Bessel function. According to Eq. (20.53) of [15], the asymptotic development of the Bessel function is

$$J_m(x) = \sqrt{\frac{2}{\pi x}}\cos\left(x - (2m+1)\frac{\pi}{4}\right) + O(x^{-3/2}). \tag{6}$$

For the geometry described in Fig. 4, the wave number change can be expressed as

$$k_\parallel = \frac{\omega}{\alpha}[\sin\theta(1+\cos\delta) + \sin\delta\cos\theta]. \tag{7}$$

Inserting Eqs. (6) and (7) into expression (5), and expanding the cosine in exponentials gives

$$F(\mathbf{k}) \propto (e^{i\pi/4}e^{i\omega T} + e^{-i\pi/4}e^{-i\omega T}), \tag{8}$$

where $T = (a/\alpha)[\sin\theta(1+\cos\delta) + \sin\delta\cos\theta]$. T and $-T$ quantify the delay time of the tip-diffraction arrivals relative to the arrival time $t = 2R/\alpha$ for a ray reflecting at the center of the fracture. Therefore, the total tip-diffraction travel times for the scattered arrival are given by Eq. (1). Note that this expression predicts a phase shift $\exp(\pm i\pi/4)$ for these waves that is characteristic of edge diffracted waves [16].

We thank ConocoPhillips for funding this research, Paul Martin for his valuable suggestions, and Randy Nuxoll for his help with sample preparation.

*tblum@cgiss.boisestate.edu
†Present address: Halliburton, Houston, TX 77042, USA.

[1] H. Nakahara, H. Sato, T. Nishimura, and H. Fujiwara, Earth Planets Space **63**, 589 (2011).
[2] E. Larose, T. Planes, V. Rossetto, and L. Margerin, Appl. Phys. Lett. **96**, 204101 (2010).
[3] L. J. Pyrak-Nolte and D. D. Nolte, Geophys. Res. Lett. **19**, 325 (1992).

[4] O. Ben-David, G. Cohen, and J. Fineberg, Science **330**, 211 (2010).
[5] B. D. Thompson, R. P. Young, and D. A. Lockner, J. Geophys. Res. **114**, B02205 (2009).
[6] S. P. Gross, J. Fineberg, M. Marder, W. D. McCormick, and H. L. Swinney, Phys. Rev. Lett. **71**, 3162 (1993).
[7] T. E. Blum, K. van Wijk, B. Pouet, and A. Wartelle, Rev. Sci. Instrum. **81**, 073101 (2010).
[8] C. B. Scruby and L. E. Drain, *Laser Ultrasonics Techniques and Applications* (Taylor & Francis, London, 1990) 1st ed..
[9] C. Scholz, *The Mechanics of Earthquakes and Faulting* (Cambridge University Press, Cambridge, England, 1990).
[10] S. Roy and L. J. Pyrak-Nolte, Geophys. Res. Lett. **24**, 173 (1997).
[11] B. Gu, K. T. Nihei, L. R. Myer, and L. J. Pyrak-Nolte, J. Geophys. Res. **101**, 827 (1996).
[12] B. Masserey and E. Mazza, J. Acoust. Soc. Am. **118**, 3585 (2005).
[13] B. J. Zadler and J. A. Scales, J. Appl. Phys. **104**, 023536 (2008).
[14] T. E. Blum, R. Snieder, K. van Wijk, and M. E. Willis, J. Geophys. Res. **116**, B08218 (2011).
[15] R. Snieder, *A Guided Tour of Mathematical Methods: For the Physical Sciences* (Cambridge University Press, Cambridge, England, 2009), 2nd ed..
[16] J. Keller, Bull. Am. Math. Soc. **84**, 727 (1978).